7th International Symposium on Marine Propulsors
Smp2022, Wuxi, China, October 17-21, 2022

Design of pumpjet propulsors using RANS-based multi-objective optimization

Stefano Gaggero, Mattia Martinelli

University of Genoa
Genoa, Italy

ABSTRACT

The design of linear pumpjets is addressed through a simulation-based design optimization approach based on RANS analyses in the case of rotor/stator (i.e., post swirl) configurations, characterized by 5 rotor blades and 5 or 10 stator blades. The optimal geometries from a multi-objective optimization process aimed at maximizing the propulsive efficiency at the lowest possible cavitation inception index are compared to a reference ducted propeller with decelerating nozzle, which served as baseline during the activity. A significant increase of propulsive efficiency with a reduced risk of cavitation is observed. Fully unsteady cavitating analyses are used to assess the reliability of the design activity, which is necessary build upon some simplifying assumptions (i.e., rotor/stator coupling through a mixing plane) needed for an affordable numerical process. Detached Eddy Simulations (IDDES) are finally carried out to highlight, in addition to the performance improvements provided by the pumpjets, also the influence of the rotor/stator/nozzle interaction on the vortical structures shed by the propulsors.

Keywords

Pumpjet; Optimization; Simulation Based Design Optimization; RANSE; Cavitation;

1 INTRODUCTION

Pumpjet propulsors are a special case of ducted propellers combining to the propeller blades and nozzle an additional system of stator blades that can be placed upstream or downstream the rotating stage. In the last years, they raised lot of interests as particularly efficient propulsive systems, especially for high-speed underwater vehicles and submarines, thanks to their ability to provide high thrust under heavy loaded conditions at sensibly lower values of radiated noise. Despite early numerical studies, due to the peculiar applications of such kind of devices in the open literature there is a minimal guidance on their design, which is still mainly based on potential flow assumptions or even more simplified hydraulic analogies and charts as reviewed by Allison (1993). McCormick & Elsenhuth (1963), for instance, proposed a first attempt to design a PJP under cavitation and efficiency requirements using vortex theory for both rotor, stator and nozzle, the latter modeled as a vortex ring. Their design process started from the nozzle, which has to be aligned along with the resultant velocity due to the rotor to avoid the negative pressure peaks at the duct nose. The outcomes of this initial step served as input for the rotor and stator design, based on a lifting line method. Furuya & Chiang (1988) developed a pumpjet design theory combing a blade-through flow with a blade-to-blade flow theory to realize a slightly three-dimensional design method using streamline curvature calculations suitable to overcome the limitations of previous approaches, like the one of Bruce et al. (1974), which were based on two-dimensional data and then not appropriate to account for the risk of flow separation on the blades. Hybrid design approaches, using a combination of potential flow theories and Euler/RANSE methods were proposed as well. Kerwin et al. (1997) developed a method for the prediction and design of pumpjets, which was successfully applied to several propulsors. Huyer & Dropkin (2011) used RANSE calculations based on Fluent on a set of accelerating and decelerating nozzles to provide the necessary inputs to the lifting surface design program PBD-14, which in turn was used to design a series of rotor/stator pumpjets tailored on those specific nozzles. Michael (2009) employed the PBD-X lifting surface design code (an evolution of PBD-14) combined with the axisymmetric Euler solver MTFLOW to the same aim, i.e. to develop a hybrid numerical design procedure for pumpjet, again based on an iterative approach between solvers.

Compared to conventional propeller design, these methods suffer of poor capabilities in predicting the interactions between the various components of the propulsor. The action of the nozzle is typically accounted using the image method only, or by the effective velocity concept assuming asymmetric flow.

The rotor/stator interaction neglects the effect of viscosity on the trailing wake of rotating blades. The leakage flow in

the gap region at the tip is often heavily simplified, with consequences on the overall PJP performances. In general, there are few investigations using high-fidelity numerical calculations (as well as using systematic experimental campaigns) on the effects of design parameters on pumpjet performances that can guide the design process, and none of these calculations was used or was specifically planned for design purposes. Wang et al. (2020), for instance, analyzed several duct parameters, including camber, tip clearance and angle of attack of a post-swirling pumpjet. Similar investigations were carried out by Huang et al. (2021), which used a parametrized description of the duct in the case of a pre-swirling pumpjet to collect open water performances for a dozen of different duct configuration. Same authors analyzed also the influence of stator parameters, like the number of stator blades, their chord, the stagger, the lean and the sweep angles plus the rotor/stator spacing using the same PJP geometry. They concluded that the overall pumpjet performances were mostly affected by the stagger angle of the stator, followed by the number of blades and the chord, while other parameters like the rotor/stator spacing or the sweep angle were almost uninfluential, confirming the outcomes of Yu et al. (2020) which proposed similar analyses on the effect of stator pitch angle and chord on the unsteady fluctuating forces of the propulsor. In both cases, however, the number of tested configurations was quite limited to gather general guidelines, also considering that no constraints on delivered thrust or cavitation inception risk were considered during the performance comparison of the geometries, and that the rotor geometry remains unchanged despite the obvious different interactions with the modified stator blades. Li et al., (2021) extended these analyses to different combinations of number of rotor and stator blades, focusing the attention on the dynamics and destabilization of the leakage vortex and its interaction with the rotor blades trailing wakes and hub vortex, as well as on the unsteady fluctuating forces of the propulsive system. No substantial changes in overall performances (i.e. delivered thrust) were observed at constant blade area ratio (number of blades times chord), but also in this case the variation of fundamental parameters like rotor blades pitch and camber was neglected and the number of cases was too limited to deduce more general design guidelines.

This is the context where the application of a Simulation Based Design Optimization approach may represent a valid and effective alternative to old-fashioned design methods also for pumpjet propulsors. SBDO have been extensively applied in many engineering fields; in the case of ship hulls and propellers the literature is full of examples showing the versatility of this method, in particular when unconventional configurations out of the application limits of usual design methods were considered. Optimization based designs, indeed, allow using more accurate solvers (i.e. RANSE), not specifically developed for design purposes, in a "try-and-error" process that results particularly suitable to address constrained and multi-objective designs and for the exploitation, for instance, of flow features not accountable by traditional inviscid calculations. In the case of marine propulsors, such methods were used for the design of unconventional geometries of propeller blades and energy saving devices (Gaggero et al., 2016, Gaggero, 2020, Furcas & Gaggero, 2021) combining in some case surrogate models like Kriging and Neural Network as well as reduced order models (Gaggero et al., 2022), with direct calculations. Since pumpjets combine some of the features already addressed in previous design applications (the nozzle of ducted propellers with stators of pre- and post- swirl) in an even more complex system, the use of a SBDO seems the natural answer to the design problem of these propulsors, considering the PJP and all the mutual interactions as a whole and not simply as the (iterative) combinations of separated elements.

This is the aim of this work: explore the design capabilities of a simulation-based design optimization method in the case of pumpjets in Rotor/Stator configuration by using a dedicated parametric description of the geometry combined with mixing plane RANSE analyses and a genetic-based optimization algorithm. The objective is to realize a propulsive system capable of delivering the required thrust at the maximum possible efficiency and at the lowest possible cavitation inception index, improving the performances of a reference ducted propeller (Gaggero et al., 2012, Villa et al., 2020), As a further insight into the features of this type of propulsors, a series of detailed DES calculations is also proposed for the best-balanced configurations identified by the optimization process, to discuss some of the peculiarities, evidenced for these devices in the recent literature when designed for a specific functioning condition.

2 THE PUMPJET MODEL

2.1 Geometry and parametric description

Figure 1 gives an overview of the propulsive configuration considered in current design activity. The pumpjet is a post-swirl one, designed to recover the energy losses of the rotor slipstream by straightening the wake. In this way stator blades produce additional thrust, unloading the rotor in favor of cavitation avoidance, and balancing at the same time the rotating moment of the entire propulsor.

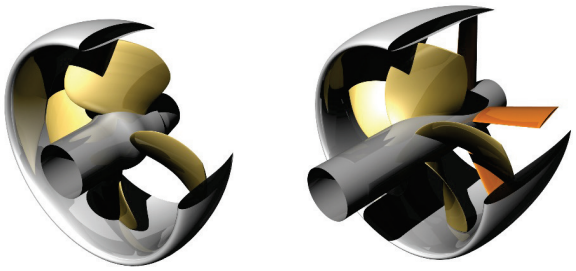

Figure 1: The reference ducted propeller and the pumpjet (5/5 configuration) considered in current design.

The system was designed to improve the performances of a reference ducted propeller which was developed in the framework of the EU funded research project BESST. This

reference is a four-bladed, controllable pitch propeller having an expanded area ratio of 0.725 and a pitch over diameter ratio at 0.7 r/R equal to 1.354. Differently from usual ducted propulsors application, this propeller was designed to operate in a decelerating duct to postpone the cavitation inception at a relatively high advance coefficient (higher than 1 and suitable, then, for a pumpjet option) since the focus was on reduction of the noise footprint of the unit rather than the maximization of the bollard pull thrust typical of accelerating ducted propulsors. The same concept of decelerating nozzle was adopted for the pumpjets design, in particular using one of the improved decelerating shapes devised in Gaggero et al. (2017).

With respect to usual pumpjets, having a large hub casing faired with the torpedo/submarine tail, the geometries of current study were developed to assess the feasibility of an optimization-based design process rather than for a specific application. For comparative purposes, they share the same hub/shaft arrangements of the reference ducted propeller and then, they are not characterized by the convergent/divergent hub/nozzle vane that typically is occupied by the stator and rotor blades. Moreover, since calculations have been carried out exploiting as much as possible the axial symmetries of the propulsors to realize a relatively efficient computational framework, working with the same (or multiple) number of blades was one of the requirements for the easy applicability of periodic boundary conditions to a reduced computational domain consisting in a blade passage only. This is the reasons behind the choice of considering 5 rotor blades combined with 5 (5/5 configuration) or 10 (5/10 configuration) stator blades in current work.

Other design parameters were selected to provide a convenient parametric description of both the rotor and the stator blades plus the nozzle (which in current analyses was handled only by the incidence angle) to be employed throughout the optimization process. The most relevant geometrical features of the blades determining the propulsor performances were defined by means of B-Spline curves. This description has provided evidence of unrivalled flexibility in enlarging the design space without losing control on the geometry using the control points as the design parameters of the optimization. Due to the complexity of the design, only radial distributions of relevant geometrical features were modified, assuming for the sectional hydrofoil shape a NACA16 thickness distribution combined with a NACA a08 camber line. Stator blades were described in terms of pitch and maximum sectional camber using, for both, a 3-points B-Spline curve, assuming a constant chord value from root to tip. For rotor blades, 4-points B-Splines were employed, and also the chord distribution was allowed to change along the blade span. A simplified distribution for the skew was added too. The resulting design space consists of 31 dimensions (parameters) listed in Table 1 that represent the independent variables of the optimization problem. Regardless the shape of rotor and stator blades, or the incidence angle of the nozzle, each pumpjet was realized with a gap (constant from the LE to the TE of the blade) between the blade tip and the internal surface of the nozzle equal 0.5% of the rotor diameter (with reference to the rotor blade plane). Any geometry was finally arranged to have a rotor/stator spacing (measured between the aftmost rotor trailing edge point and the foremost stator leading edge point) not lower than 10% the rotor diameter, even if a very reduced influence of this parameter (within certain limits) was observed in previous analyses (Huang et al., 2021).

Table 1. Range of variation of pumpjet design parameters.

parameter	range	parameter	range
$p/D_{1\,stat.}$	0 – 1.5	$p/D_{1\,rot.}$	0.7 – 1.5
$p/D_{2\,stat.}$	0 – 2	$p/D_{2\,rot.}$	0.8 – 1.9
$p/D_{3\,stat.}$	0 – 2	$p/D_{3\,rot.}$	0.8 – 1.9
$r/R\ p/D_{2\,stat.}$	0.4 – 0.8	$p/D_{4\,rot.}$	0.7 – 1.6
$f/c_{1\,stat.}$	-0.05 – 0.05	$r/R\ p/D_{2\,rot.}$	0.3 – 0.6
$f/c_{2\,stat.}$	-0.05 – 0.05	$r/R\ p/D3_{\,rot.}$	0.65 – 0.9
$f/c_{3\,stat.}$	-0.05 – 0.05	$c/D_{1\,rot.}$	0.15 – 0.4
$r/R\ f/c_{2\,stat.}$	0.3 – 0.8	$c/D_{2\,rot.}$	0.2 – 0.55
$c/D_{\,stat.}$	0.1 – 0.2	$c/D_{3\,rot.}$	0.2 – 0.55
Duct angle	-5° – 5°	$c/D_{4\,rot.}$ ($\%c/D_{3\,rot.}$)	10% – 100%
$sk_{2\,rot.}$	-10° – 5°	$r/R\ c/D_{2\,rot.}$	0.3 – 0.6
$sk_{3\,rot.}$	0° – 15°	$r/R\ c/D_{3\,rot.}$	0.65 – 0.98
$r/R\ sk_{2\,rot.}$	0.3 – 0.8	$f/c_{1\,rot.}$	-0.05 – 0.05
		$f/c_{2\,rot.}$	-0.05 – 0.05
		$f/c_{3\,rot.}$	-0.05 – 0.05
		$f/c_{4\,rot.}$ ($\%\,f/D_{3\,rot.}$)	10% – 90%
		$r/R\ f/c_{2\,rot.}$	0.3 – 0.6
		$r/R\ f/c_{3\,rot.}$	0.65 – 0.95

2.2 Numerical models

The design process and the unsteady analyses of the final configurations rely on different numerical models and associated computational domains. The need of computationally efficient calculations for the thousands of analyses required in the design process imposes some simplification to the computational model, that is built using turbomachinery analogies, in particular exploiting the "mixing plane" approach which is a technique typically used to compute steady-state simulations of coaxial multi-stage systems. Instead of the fully unsteady analyses needed for time-resolved solutions of the flow across stages moving relative to one another, in correspondence of this mixing plane interface, opportunely placed between the stages (Fig. 2), the circumferentially averaged flow field is transferred in a conservative manner between two rotationally regions aligned on the same axis. Mass, momentum, energy, and other conserved quantities are averaged in concentric, circumferential rings of uniform radial thickness covering the entire interface boundary. Due to this averaging process, the final solution is characterized by radially varying profiles of flow quantities that remain uniform along the circumferential direction within any given circumferential ring, allowing for steady calculations in a sort of "equivalent" inflow. Together with periodic boundary conditions, the computational domain is reduced to a single blade passage consisting of two coaxial regions, matched by the mixing plane itself. The

calculations are steady, since moving reference frame is applied in the rotor region, providing in this way a computationally efficient estimation of the averaged performances of the propulsor.

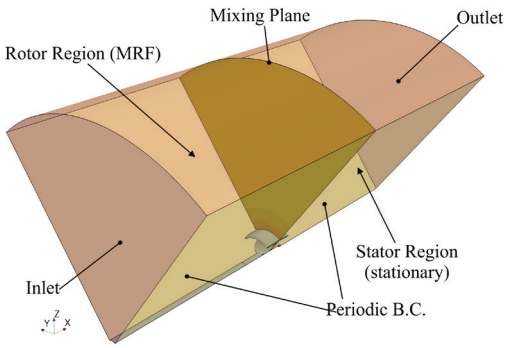

Figure 2: Computational domain for "mixing plane" analyses of the optimization process.

This problem was addressed using RANS equations, solved on an unstructured polyhedral mesh of about 1 million cells using the finite volume solver StarCCM+ (Siemens, 2020) and the SST k-ω turbulence model.

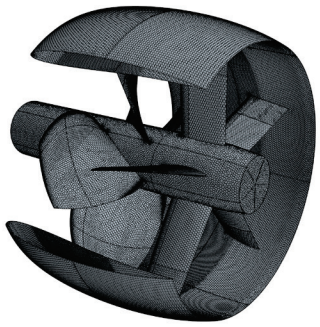

Figure 3: Surface grid on the pumpjet (5/5 configuration).

Fully unsteady analyses, using sliding meshes, were additionally carried out for a twofold objective. At first, to verify, in the case of a set of optimal configurations, the reliability of the simplifications accepted in the design process. To this aim fully unsteady RANSE analyses in both non-cavitating (i.e. reliability of the "mixing plane" assumption) and cavitating conditions (i.e. reliability of the simplified cavitation inception criteria) were considered. Meshes, again of polyhedral type, counted up to 9 million cells. An example of calculation for a representative geometry of a 5/5 configuration is given in Fig. 4. The "mixing plane" calculation show quite limited differences to time resolved calculations. The pressure distribution over rotor and stator blades is very similarly predicted, allowing reliable estimation of the risk of cavitation inception using the simplified calculation setup. Some differences can be appreciated on the external surface of the nozzle, in correspondence of the mixing plane interface where the averaging process slightly affects the flow field across the boundary layer of the duct. Stator blades that are subjected to the rotor slipstream, and then to unsteady flow, show the most relevant differences.

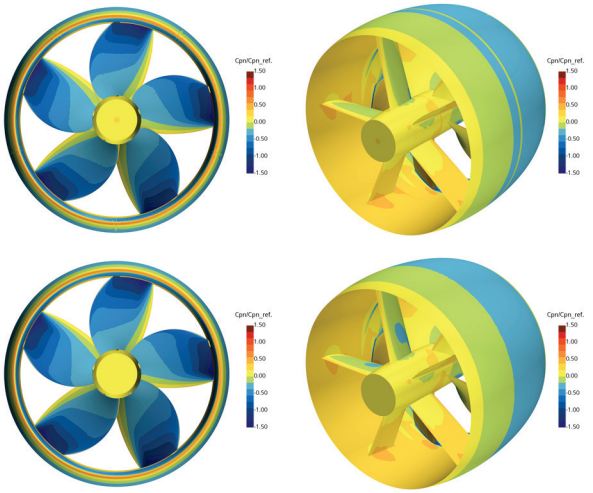

(a) Back side (rotor) (b) Face side (rotor and stator)

Figure 4: Comparison between mixing plane (top) and truly unsteady (bottom, key blade at 0 deg.) RANSE analyses. Normalized pressure coefficient ($C_{PN}/\sigma_{Ndesign}$) at the design advance coefficient of a representative R/S pumpjet configuration.

They are ascribable to the complex and non-homogeneous flow field from rotor blades, at that simulation step (i.e. stator/rotor relative position), compared to the circumferentially averaged velocity field of the mixing plane analyses. In terms of propulsive performances, the "mixing plane" analyses differ less than 2% with respect to the fully unsteady case, at least for all the relevant quantities (total delivered thrust, absorbed torque and efficiency) used in the design process.

Fully unsteady analyses, secondly, were considered to assess the influence of the mutual rotor/stator/nozzle interactions on the evolution/destabilization of the trailing vortical wake. For this, IDDES analyses were considered and compared to results of the reference ducted propeller. In this case some specific zonal refinements were used, in particular encompassing the nozzle wake where the most significant dynamics of trailing vortexes are expected, rising the cell count to up to 30 million.

In both cases the time step was set equivalent to 0.5 deg. of propeller rotation using a second order implicit discretization scheme. Second order schemes were also used for the convective terms, coupling velocity and pressure with the SIMPLE scheme under the segregated flow assumption.

2.3 Optimization workflow

The design of pumpjet propulsors using simulation-based design optimization approaches is not different to what has been already proposed for conventional propellers. However, the use of RANSE calculations in place of BEM analyses to accurately account for mutual rotor/stator/nozzle interactions, barely addressed by potential flow analyses, suggests some additional strategies to deal with a complex multi-objective constrained optimization problem. To this aim, the non-cavitating, dual

step procedure devised for the design of RIM-driven propellers in Gaggero (2020), has been identically applied to this design case.

Rather than monitoring the portion of the rotor (or stator) blades covered by vapor, the minimization of the pumpjet cavitation has been pursued by monitoring the cavitation inception risk, more easily obtainable by non-cavitating and computationally efficient steady calculations. From a mere cavitation free design, the cavitation inception has to be avoided anywhere. Then, the minimization of the highest suction peak on the entire propeller blade could be considered the only design objective. But collecting data at different blade locations provides a more detailed characterization of the phenomena occurring on the propeller, which could be useful for a better understanding and for a reasoned selection of the "optimal" design among the Pareto configurations. To this aim, both rotor and stator blades are subdivided in several zones over which pressure data are sampled and processed. In particular, in order to distinguish (the risk of) sheet and bubble cavitation, leading edge ("LE", $0<x/c<0.1$) and midchord ("MID", $0.1<x/c<0.6$) locations, at tip and at the root of the blades, on both back and face side of rotor and stator are collected separately and used as design objectives of the optimization process.

Moreover, not all the configurations progressively identified by the optimization process are required to be solved up to the maximum number of iterations needed for the numerical convergence of the RANSE calculation. The really important ones are those that reasonably will satisfy the design constraints (in this case, the thrust), and they can be identified by monitoring intermediate values of the key performance indicators used in the optimization process. In this specific case, a loosened tolerance on the total delivered thrust (±4%) is used to accept the case as potentially feasible (and then to continue calculations up to numerical convergence) or to reject it and use it as a penalizing objective.

The resulting optimization problem for the design of pumpjet propulsors consists then in a constrained multi-objective optimization carried out in a 31-dimension design space where the maximization of the propulsive efficiency is accomplished under a given thrust (±1.5% of tolerance) and with the minimum risk of cavitation inception through the minimization of the pressure peaks collected in the various zones of the blades. The problem, with six design objectives and one constraint, is handled in modeFrontier (Esteco, 2017), using its MOGA-II genetic algorithm starting from an initial population of 620 (20 times the design parameters) configurations. Both the designs (5/5 and 5/10 configuration) ended after 15 evolutions of the initial samples of the design space, evaluating a total of 9300 different geometries per design case.

3 RESULTS AND DISCUSSION

The results of the two optimization processes are collected in the parallel diagrams of Figs. 5~6 that show, for all the feasible propellers satisfying the thrust constraint, the performance indexes describing their efficiency and their cavitating behavior. The key performance indicators of the ducted propeller are given as well to serve as reference for the selection of the optimal propulsors.

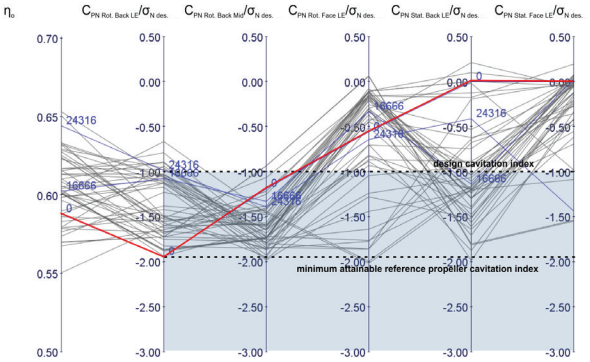

Figure 5: Parallel plot of configuration 5/5. Cases filtered with a minimum normalized cavitation index set to 2.

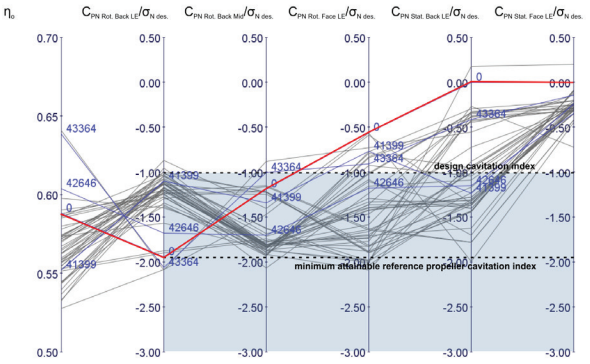

Figure 6: Parallel plot of configuration 5/10. Cases filtered with a minimum normalized cavitation index set to 2.10.

As thoroughly discussed in several papers the use of a decelerating nozzle substantially improves the margin against cavitation of the ducted propeller, that is affected by a consistent risk of cavitation only at the tip of the blade and across the gap (then at midchord), where the development of a leakage vortex determines, locally, values of suction higher than the design cavitation index. The distribution of the performance indexes of the analyzed PJP geometries, regardless their configuration, clearly show a certain difficulty in designing a propulsors having better cavitation performance than the reference propeller, especially for what concern suction side leading edge phenomena on the rotor blades. In both cases, there are very few geometries capable of increasing the inception speed of the reference configuration, maintain at the same time decent performances on the pressure side or on the stator blades. Pumpjets, indeed, suffer of the same issues of ducted propulsors in the tip region, where the cross-flow and the interaction with the boundary layer of the inner nozzle surface have the highest influence on the pressure distribution over the rotor blades. From the efficiency point of view PJPs show their potentialities, since there are

several configurations capable of ensuring substantially higher values of efficiency that, for instance, were not possible in the case of equivalent RIM driven (Gaggero, 2020) due to the parasitic torque of the rim itself.

Based on these results, a selection criterion consisting in the complete avoidance of cavitation ($C_{PN}/\sigma_{Ndesign} > -1$) with the maximum possible efficiency would result useless, since none of the geometries analyzed in the process permits such performances. The overall bests, then, are those that provide the highest inception speed everywhere on the rotor and stator blades. They can be selected by reducing simultaneously the threshold on the cavitation index for the five performance indicators ($C_{PN\ Rot.\ Back\ LE}$, $C_{PN\ Rot.\ Back\ MID}$, $C_{PN\ Rot.\ Face\ LE}$, $C_{PN\ Stat.\ Back\ LE}$, $C_{PN\ Stat.\ Face\ LE}$) maintaining as high as possible the propulsive efficiency.

For the 5/5 configuration, the first feasible geometries are possible with a threshold on the cavitation inception equal to 1.5 times the design cavitation index. This choice identifies 5/5-16655 and 5/5-24316 as two possible optimal configurations. They have the same inception speed ($C_{PN}/\sigma_{Ndesign}$ of about 1.4, occurring at the midchord tip of the suction side of the rotor) but with different cavitating phenomena on the stator. One of the two (5/5-24316) has one of the highest possible efficiencies identified during the design process.

Compared to the reference ducted propeller, leading edge inception on the back side is substantially postponed, since both geometries realize a $C_{PN}/\sigma_{Ndesign}$ close to -1. Improvements at midchord, as discussed, are hardly feasible due to the similarities of pumpjet propulsors with conventional ducted propellers in terms of leakage flow and associated vortical structures on the tip of the blade (which are confirmed by the truly cavitating analyses on the set of optimal geometries of Fig. 9). A longer nozzle, actually, could additionally worsen the interactions with the rotor. Most of the geometries with reasonable margins on the leading-edge show, indeed, higher values of suction at midchord. The pressure distributions of Fig. 7 illustrate these features. The inception is anticipated to the 130% of the design cavitation index (120% for the ducted propeller), with particularly low and extended values of suction on the trailing part of the blade at tip. On the pressure side of the rotor improvements are not outstanding compared to the reference geometry but, in any case, the inception is well below (30 to 60%) the design cavitation index, preventing any possible issue also for the pumpjets. Stator blades, on the contrary, suffer from cavitation inception at relatively higher cavitation indexes. This is particularly true for 5/5-24316, which exhibits the risk of leading-edge cavitation at about 140% of the design condition. On the contrary, both the selected pumpjets provide significantly higher values of propulsive efficiency. 5/5-16666, which in the end is the overall most conservative choice from the cavitation risk point of view realizes an efficiency 1.5% higher than the ducted propellers; 5/5-24316 increases the improvement up to 6%.

Similar results are achieved by the 5/10 pumpjet configuration. In this case the first feasible geometry has a threshold on the cavitation inception equal to 1.4 times the design cavitation index. This geometry, 5/10-41399, however, realizes an overall propulsive efficiency 3.5% lower than that of the reference ducted propeller. Among geometries having an efficiency higher than that of the reference, there are only few candidates with cavitation inception better that the original ducted propeller. Setting the limit to the "minimum reference propeller attainable cavitation index" ($C_{PN}/\sigma_{Ndesign}$ = -1.96, leading edge at tip for the reference ducted propeller), 5/10-42646 is the pumpjet with the highest efficiency (+1.5%) but serious anticipation of the cavitating phenomena at midchord, since the cavitation index is equal to 1.7 times the design one versus a reference propeller having the risk of midchord cavitation equal to 1.25 the design value. This confirms the difficulty of achieving significant improvements at midchord as a combination of leakage flow in the gap and longer nozzles.

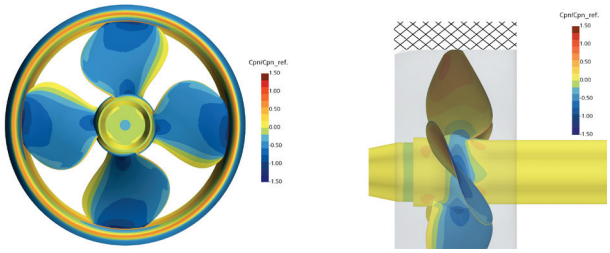

(a) Reference ducted propeller

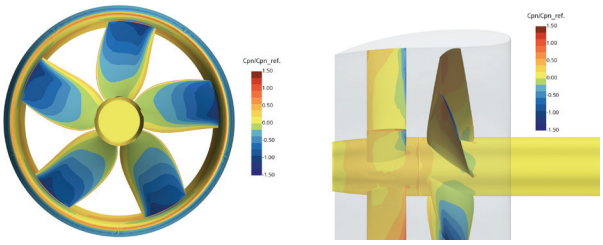

(b) 5/5-24346

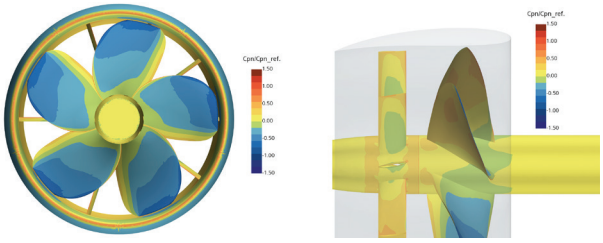

(c) 5/10-43364

Figure 7: Normalized pressure distribution ($C_{PN}/\sigma_{Ndesign}$, mixing plane analyses) on the optimal pumpjets. Comparison with the reference ducted propeller. For confidentiality reasons the reference decelerating nozzle has been hidden.

Accepting, instead, a negligible worsening of the leading-edge performances at tip ($C_{PN\ Rot.\ Back\ LE}/\sigma_{Ndesign}$ = 2.05), pumpjet 5/10-43364 appears as a very interesting compromise. Midchord cavitation is reduced and also cavitating phenomena on the stator blades, as well as those on the pressure side at leading edge of the rotor are almost

negligible compared to the design functioning point. Moreover, the increase of efficiency provided by this geometry is higher than 5%. Together with 5/5-24316, this is the geometry selected for detailed unsteady analyses, including cavitation prediction and wake dynamics using IDDES calculations.

The unsteady calculations, for a relatively large range of advance coefficients, are shown in Fig. 8. As already observed for the representative pumpjet geometry of Fig. 4, the unsteady analyses confirm the results of the optimization process for both the 5/5 and the 5/10 configurations, which moreover are ranked similarly (5/5 slightly better, in terms of propulsive efficiency, than 5/10) also when solving the rotor/stator interactions with the unsteady approach. The predicted efficiency is even higher, and the improvements granted by both the pumpjets are close to 7%.

With the same grid arrangement, the cavitating analyses of Fig. 9, carried out with the homogeneous mixture assumption and the Schnerr-Sauer mass transfer model using the same, relatively coarse, grid arrangement confirms the outcomes of the optimization process and of the simplified indicators of cavitation adopted throughout the design.

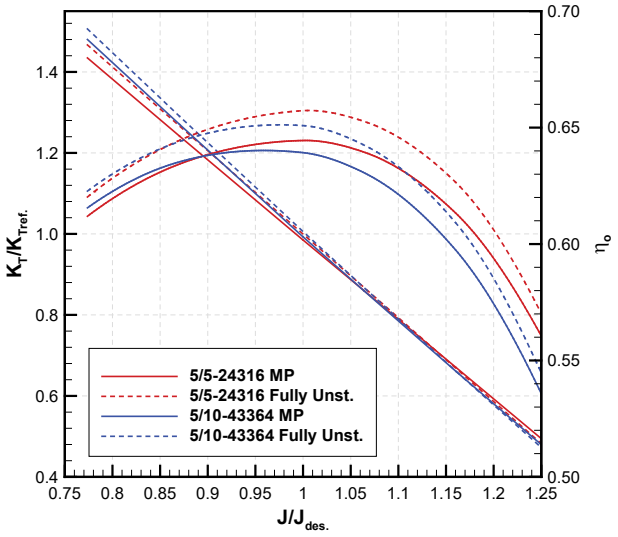

Figure 8: Pumpjets performances. Comparison between mixing plane calculations (MP, solid line) and fully unsteady RANSE calculations (Fully Unst., dashed line)

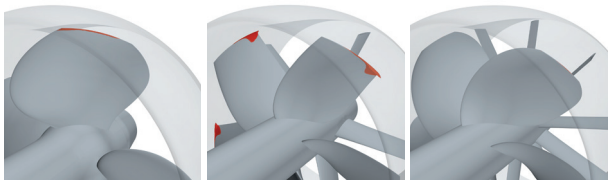

Figure 9: Predicted cavitation (RANSE with homogeneous mixture/VoF approach) on the reference ducted propeller (left), 5/5-24316 (middle) and 5/10-43364 (right)

In the case of the reference ducted propeller the only appreciable phenomenon is a cavitating leakage vortex, in this case under resolved due to insufficient grid density (see, for instance, calculations in Gaggero et al., 2014 for detailed numerical predictions and comparisons with experiments), starting at the leading edge of the blade in accordance with the minimum of the pressure coefficient discussed in Fig. 7 and in the parallel diagrams of the optimization process. Pumpjets 5/5-24316 and 5/10-43364 show, instead, very different behaviors. As expected, in the case of the 5/5 configuration, the most evident phenomenon is the presence of midchord cavitation extended on a relatively large portion of the blade at the tip. Pumpjet 5/10-43364, instead, with this choice of computational grid is almost cavitating free since there is only a hardly identifiable cavitating leakage vortex in the tip/nozzle gap and the very low value of suction observed during the optimization process at the leading edge of the blade (Fig. 6) is not sufficiently extended to sustain an appreciable vaporization process. This suggests the need of

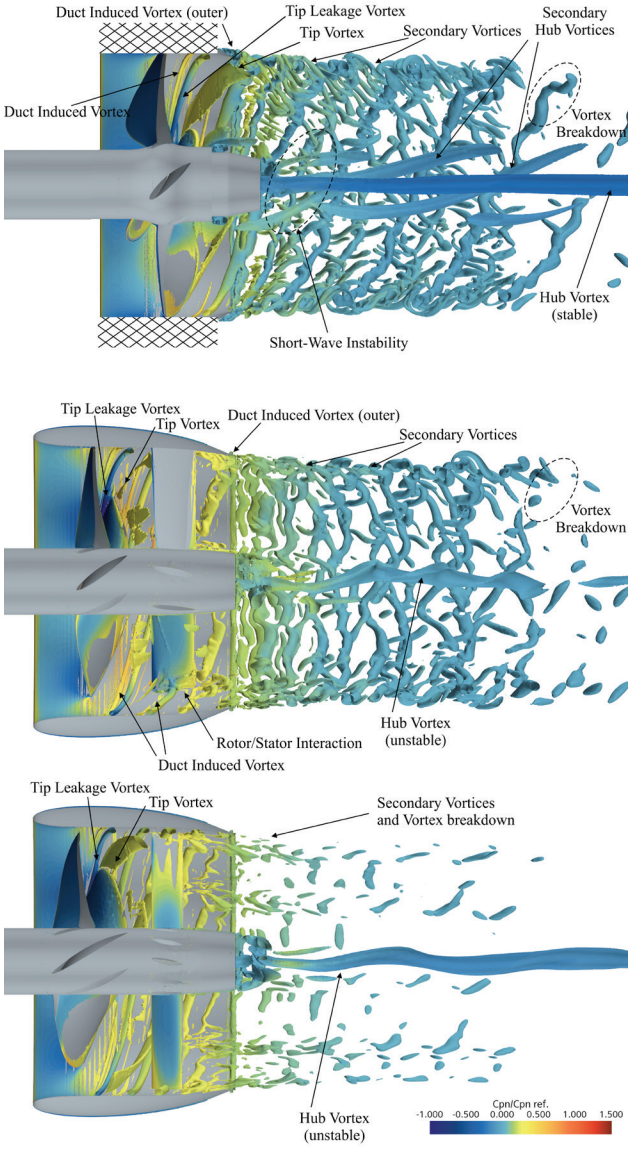

Figure 10: Vortical structures (isosurface of Q = 10000 s^{-2}, IDDES analyses) in the wake of the propulsors. Snapshot after 18 propeller revolution. For confidentiality reasons the reference decelerating nozzle has been hidden.

controlling with improved performance indicators the occurrence of cavitation in the design process. The dynamics of the trailing vortical wakes is finally analyzed by means of IDDES calculations. Compared to similar analyses available in literature (Qin et al., 2021, Huang et al., 2021 among the others) current geometries (of the pumpjets as well as of the reference ducted propeller) were designed for the same functioning conditions and with the same criteria (reduction of the risk of cavitation).

This means that for the required delivered thrust only the best-balanced configurations are available, avoiding for instance design solutions that compensate an excessive nozzle drag with a higher rotor thrust and, in turn, the serious risk of boundary layer separation on the duct that proved to hasten the triggering of wake instability. Consequently, they represent a set of configurations for "fair" comparisons also in terms of wake evolution and destabilization. The vortical structures developed by the reference ducted propeller are shown in Fig. 10 using an instantaneous surface of Q = 10.000 s^{-2} taken after 18 propeller revolutions. Inside the nozzle it is easy to recognize the tip leakage vortex, which is the most relevant vortical structure shed by the blade tip, placed side by side to secondary structures comparable to the "duct induced vortexes" evidence in Qin et al. (2021). Similar structures, already evidenced by RANSE (Villa et al., 2020) are visible also on the outer ducted surface, very close to its trailing edge. With respect to the analyses of Qin (Qin et al, 2021), current propeller is working at the design point, with the duct aligned to the inflow, then with a minimum risk of flow separation that makes these vortices almost negligible and confined to the trailing edge only. Inside the nozzle also the blade trailing wake is easily recognizable with a helical pitch significantly higher than that of the leakage vortex, decreased by the interaction with the internal boundary layer of the nozzle. The instability of the trailing wake, however, seems triggered in a very different way to what concluded using only RANSE analyses (Villa et al., 2020). Among the most common instability inception phenomena, the mutual inductance instability mode (Widnall, 1974), or "leapfrogging", observed in many conventional propellers between and as a function of the distance of adjacent vortical helical filaments (then of the advance coefficient) is the usual reason of propeller tip vortex instability. RANSE analyses of Villa et al. (2020) evidenced a similar interaction between the tip leakage vortex and the additional vortical structures shed by the duct at a certain distance from the duct itself, where vortices finally merged into thicker structures. Current analyses, instead, highlight a much more complex interaction that in the end nullify the stable region of the propulsor wake, since the short-wave instability, i.e. the small sinusoidal displacements of every vortical filament (Widnall, 1974), is early observable on the coherent vortical structures emanating from the tip of the blades. As observed by Gong et al. (2018) there are several and intense secondary vortical structures wrapped around the tip vortices, bridging the vortices of subsequent blades and then promoting the mutual induction. Even if observed also for conventional open propeller in high-load functioning conditions, in current case these secondary vortical structures mainly rise from the interaction of the duct induced vortices and the tip leakage vortex of the blade: vortices shed from the duct connect with the tip leakage vortices starting a rolling-up and wrapping process that originates these secondary structures, realizing the "tip-duct mutual inductance instability" of Qin et al. (2021). From this point of view, it is the shear layer of the duct that plays the most important role in the destabilization process of the wake. The boundary layer formed on the walls of the duct (like in the case of airfoils) is shed in the wake, but it is disturbed by the presence of the helical vortices (tip or tip leakage) from the blades. This mutual interaction leads to the turbulence kinetic energy disturbance of the tip vortex and to the development of the duct shear layer into the duct induced vortices which mutual influence distorts the tip/leakage vortex and generates the secondary structures. IDDES analyses highlight also a certain trailing wake/tip vortex interaction in addition to the usual spiral-to-spiral mutual inductance interaction. The roll-up process of the blade trailing wake, described in Kumar & Mahesh (2017), is observable too. The trailing vortical wake of the ducted propeller blades withstands a tangential and radial deformation induced by the opposite strength of trailing vortices depending on their radial (root or tip) position. This turns into an "approaching" of the outer portion of the trialing wake to the tip leakage and duct induced vortices, promoting an additional interaction and further destabilization influences. The hub vortex, on the contrary, seems to have a prevalent stable nature since only negligible oscillations are visible also at a certain distance from the boss cap. A coherent structure made of four secondary root blade vortices, and promoted also by the shape of the hub of the ducted propeller, is present as well but its influence on the dynamic of the hub vortex seems marginal.

The pumpjet configuration determines a substantial change in the dynamic of the trailing wake of the propulsors, which definitely loses (especially in the 5/10 setup) any of the coherent structures observed, at least partially, for the tip/leakage vortex of the reference propeller. As for the ducted propeller, for this selection of optimal pumpjets the tip/duct mutual inductance seems the most important trigger to wake instability being, moreover, the shear layer of the nozzle stronger, if compared to the reference propeller, as a consequence of the longer duct adopted for pumpjets. The structure of the tip vortices when inside the nozzle, indeed, is very similar to what observed in the case of the reference ducted propeller. A non-negligible leakage vortex developed in the clearance between the rotor tip and the nozzle is visible, together with some minor duct-induced vortices on its inner surface. Those on the outer side of the nozzle have a negligible importance, thanks to the adjustment of the nozzle incidence provided by the optimization design. Their interaction with the duct shear layer produces a wake in which a stable (or at least

transition) behavior is substantially absent. The resulting wake is a shear layer vortex sheet fully mixed with the rotor tip vortices already downstream the duct trailing edge, forming a sort of "flat" cylindrical surface of vorticity, made of a series of spiral filaments attached each other in place of independent helical structures, well visible in Figs. 10~11. Increasing the number of stator blades exacerbates this phenomenon. Each stator blade "breaks" several times the tip rotor vortices producing additional secondary vortices that, in turn, are subjected to a mixing process with the intense shear layer of the nozzle. The result, in the case of the 5/10 configuration is a completely uncoherent wake (i.e. without any residual shade of independent helical structures) fully mixed with the nozzle shear layer. Hub vortexes behave very differently.

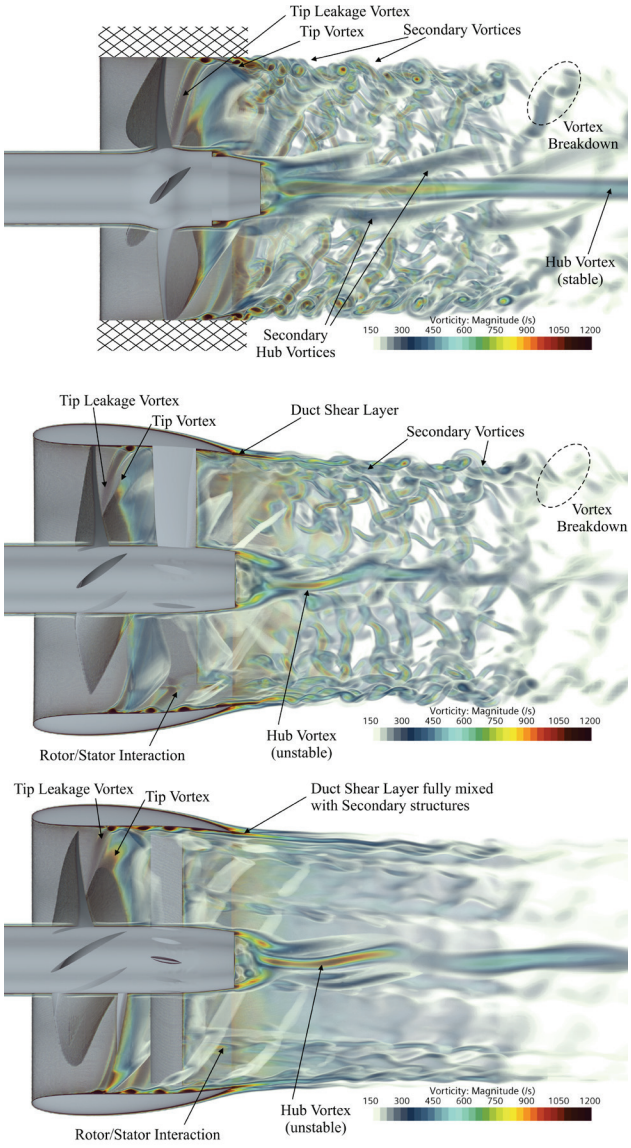

Figure 11: Volume vorticity (IDDES analyses) in the wake of the propulsors. Snapshot after 18 propeller revolution. For confidentiality reasons the reference decelerating nozzle has been hidden.

This can be ascribed to the different blade load distributions obtained through the design process. 5/5-24316, for instance, has a quite intense hub vortices that, however, undergoes a very early destabilization as a reasonable consequence of the interaction with the secondary vortices rotating around the hub. Hub vortex of 5/10-43364, instead, resembles that of the reference propeller, maintaining its stable nature regardless the interaction with the post-swirl stator blades.

4 CONCLUSIONS

In current work, the design of pumpjet propulsors was addressed using a simulation-based design optimization framework. It consists in a custom parametric description of both rotor and stator blades and a genetic algorithm working with viscous RANSE analyses that are needed to (partially) address the complexity of the mutual rotor/stator/nozzle interactions. A 31-dimension design space, built using the B-Spline control points of the curves describing the geometry of the propulsor, is used to enlarge the exploration range of the optimization process while RANSE analyses exploit periodic boundary conditions and "mixing plane" interfaces to realize a simplified, but reliable and computationally efficient, simulation environment. Different rotor/stator configurations are considered to generalize the design process that is formulated as the maximization of the propulsive efficiency constrained to a given delivered thrust and with the minimum possible risk of cavitation. A decelerating nozzle configuration, adapted from previous design activities but less common for this type of applications (apart from submarines), has been used since cavitation avoidance was considered a primary goal of the new propulsors design. Optimized pumpjets provide substantial performances improvement, close to a 6% of propulsive efficiency increase with limited/nullified cavitation. The complex interactions of tip and trailing vortical wakes of nozzle, rotor and stator have been finally investigated using IDDES analyses. They evidenced massive secondary structures fostering the destabilization of the wake and the mixing, in a non-coherent structure, of the vortexes from the rotor blades with the shear layer of the nozzle. This was particularly evident when the highest number of stator blades (10) was employed.

REFERENCES

Allison, J.L. (1993). 'Marine waterjet propulsion'. Trans. Of SNAME, **101**, pp. 275-335.

Bruce, E. P., Gearhart, W. S., Ross, J. R., & Treaster, A. L. (1974). 'The design of pumpjets for hydrodynamic propulsion'. Fluid Mech., Acoustics, and Design of Turbomachinery, NASA SP-304.

Esteco (2017). modeFRONTIER Users' Manual.

Furcas, F., & Gaggero, S. (2021). 'Pre-swirl stators design using a coupled BEM-RANSE approach'. Ocean Engineering, **222**, 108579.

Furuya, O., & Chiang, W. L. (1988). 'A new pumpjet design theory'. DTIC Document.

Gaggero, S., Rizzo, C. M., Tani, G., & Viviani, M. (2012). 'EFD and CFD design and analysis of a propeller in

decelerating duct'. International Journal of Rotating Machinery, 2012.

Gaggero, S., Tani, G., Viviani, M., & Conti, F. (2014). 'A study on the numerical prediction of propellers cavitating tip vortex'. Ocean Engineering, **92**, 137-161.

Gaggero, S., Gonzalez-Adalid, J., & Sobrino, M. P. (2016). 'Design and analysis of a new generation of CLT propellers'. Applied Ocean Research, **59**, 424-450.

Gaggero, S., Villa, D., Tani, G., Viviani, M., & Bertetta, D. (2017). 'Design of ducted propeller nozzles through a RANSE-based optimization approach'. Ocean Engineering, **145**, 444-463.

Gaggero, S. (2020c). 'Numerical design of a RIM-driven thruster using a RANS-based optimization approach'. Applied Ocean Research, **94**, 101941.

Gaggero, S., Vernengo, G. & Villa, D. (2022). 'A marine propeller design method based on two-fidelity data levels'. Applied Ocean Research, **123**, 103156.

Gong, J., Guo, C. Y., Zhao, D. G., Wu, T. C., & Song, K. W. (2018). 'A comparative DES study of wake vortex evolution for ducted and non-ducted propellers'. Ocean Engineering, **160**, 78-93.

Huang, Q., Li, H., Pan, G., & Dong, X. (2021). 'Effects of duct parameter on pump-jet propulsor unsteady hydrodynamic performance'. Ocean Engineering, **221**, 108509.

Huyer, S. A., & Dropkin, A. (2011). 'Integrated motor/propulsor duct optimization for increased vehicle and propulsor performance'. Journal of Fluids Engineering, **133**(4).

Kerwin, J. E., Taylor, T. E., Black, S. D., and McHugh, G. P. (1997). 'A coupled lifting-surface analysis technique for marine propulsors in steady flow'. SNAME Propellers/Shafting '97 Symposium,Virginia Beach, VA.

Kumar, P., & Mahesh, K. (2017). 'Large eddy simulation of propeller wake instabilities'. Journal of Fluid Mechanics, **814**, 361-396.

Li, H., Huang, Q., Pan, G., Dong, X., & Li, F. (2021). 'Effects of Blade Number on the Propulsion and Vortical Structures of Pre-Swirl Stator Pump-Jet Propulsors'. Journal of Marine Science and Engineering, **9**(12), 1406.

McCormick, B. W., & Elsenhuth, J. J. (1963). 'Design and performance of propellers and pumpjets for underwater propulsion'. AIAA Journal, **1**(10), 2348-2354.

Michael, T. J., Schroeder, S. D., & Becnel, A. J. (2008). 'Design of the ONR AxWJ-2 axial flow water jet pump'. Naval Surface Warfare Center Carderock Division, Report NSWCCD-50-TR-2008/066

Qin, D., Huang, Q., Shi, Y., Pan, G., Shi, Y., & Dong, X. (2021). 'Comparison of hydrodynamic performance and wake vortices of two typical types of pumpjet propulsor'. Ocean Engineering, **224**, 108700.

Siemens, P.L.M. (2020). StarCCM+ Users' Manual, V. 15.06. Siemens PLM.

Villa, D., Gaggero, S., Tani, G., & Viviani, M. (2020). 'Numerical and experimental comparison of ducted and non-ducted propellers'. Journal of Marine Science and Engineering, **8**(4), 257.

Wang, C., Weng, K., Guo, C., Chang, X., & Gu, L. (2020). 'Analysis of influence of duct geometrical parameters on pump jet propulsor hydrodynamic performance'. Journal of Marine Science and Technology, **25**(2), 640-657.

Widnall, S. E. (1972). 'The stability of a helical vortex filament'. Journal of Fluid Mechanics, **54**(4), 641-663.

Yu, H., Duan, N., Hua, H., & Zhang, Z. (2020). 'Propulsion performance and unsteady forces of a pump-jet propulsor with different pre-swirl stator parameters'. Applied Ocean Research, **100**, 102184.